Disagreement on the North Atlantic Cold Blob Formation Mechanisms among Climate Models

YIFEI FAN,[a] DUO CHAN,[b] PENGFEI ZHANG,[a] AND LAIFANG LI[a,c,d]

[a] *Department of Meteorology and Atmospheric Science, The Pennsylvania State University, University Park, Pennsylvania*
[b] *School of Ocean and Earth Science, University of Southampton, Southampton, United Kingdom*
[c] *Institute of Computational and Data Sciences, The Pennsylvania State University, University Park, Pennsylvania*
[d] *Earth and Environmental Science Institute, The Pennsylvania State University, University Park, Pennsylvania*

(Manuscript received 27 October 2023, in final form 7 March 2024, accepted 10 April 2024)

ABSTRACT: Despite global warming, the sea surface temperature (SST) in the subpolar North Atlantic has decreased since the 1900s. This local cooling, known as the North Atlantic cold blob, signifies a unique role of the subpolar North Atlantic in uptaking heat and hence impacts downstream weather and climate. However, a lack of observational records and their constraints on climate models leave the North Atlantic cold blob formation mechanism inconclusive. Using simulations from phase 6 of Coupled Model Intercomparison Project, we assess the primary processes driving the North Atlantic cold blob within individual models and whether the mechanisms are consistent across models. We show that 11 out of 32 models, which we call "Cold Blob" models, simulate the subpolar North Atlantic cooling over 1900–2014. Further analyzing the heat budget of the subpolar North Atlantic SST shows that models have distinct mechanisms of cold blob formation. While 4 of the 11 Cold Blob models indicate decreased oceanic heat transport convergence (OHTC) as the key mechanism, another four models suggest changes in radiative processes making predominant contributions. The contribution of OHTC and radiative processes is comparable in the remaining three models. Such a model disagreement on the mechanism of cold blob formation may be associated with simulated base-state Atlantic meridional overturning circulation (AMOC) strength, which explains 39% of the intermodel spread in the contribution of OHTC to the simulated cold blob. Models with a stronger base-state AMOC suggest a greater role of OHTC, whereas those with a weaker base-state AMOC indicate that radiative processes are more responsible. This model discrepancy suggests that the cold blob formation mechanism diagnosed from single model should be interpreted with caution.

SIGNIFICANCE STATEMENT: The mechanisms driving sea surface temperatures over the subpolar North Atlantic to cool since the 1900s remain uncertain due to the lack of direct observations. Here, we use a temperature change decomposition framework to dissect the historical trend of surface temperature simulated in multiple global climate models. The models diverge on whether the subpolar North Atlantic cooling is induced by reduced ocean heat transport convergence or altered radiative processes. Notably, the importance of ocean heat transport convergence is influenced by the simulated base-state strength of Atlantic meridional overturning circulation and the Irminger Sea's mixed layer depth. This finding cautions against concluding the cooling mechanism from a single model and highlights a need for ongoing observations to constrain AMOC-related climate projection in the subpolar North Atlantic.

KEYWORDS: Feedback; Meridional overturning circulation; Sea surface temperature; Air–sea interaction; Climate change

1. Introduction

Running counter to global warming since the Industrial Revolution, the sea surface temperature (SST) in the subpolar North Atlantic has decreased in the past century at a rate of 0.39 (±0.23, 95% confidence interval) K century^{-1} (Li et al. 2022; Drijfhout et al. 2012; Kim and An 2013; Rahmstorf et al. 2015). This phenomenon, predominantly observed to the southeast of Greenland, is known as the North Atlantic cold blob[1]. The presence of the North Atlantic cold blob underscores the subpolar North Atlantic's distinctive role in heat uptake and redistribution in response to anthropogenic forcing (Winton et al. 2013; Marshall et al. 2015). By influencing local SST, the meridional SST gradient, ocean stratification, and air–sea coupling, the North Atlantic cold blob has significant climate impacts, including but not limited to the location and spatial extent of the North Atlantic storm track (Woollings et al. 2012), European temperature and precipitation patterns (Haarsma et al. 2015; Gervais et al. 2020), the latitude of the

Supplemental information related to this paper is available at the Journals Online website: https://doi.org/10.1175/JCLI-D-23-0654.s1.

Corresponding author: Laifang Li, lfl5240@psu.edu

[1] We acknowledge that "warming hole" is more commonly used to describe the lack of arming in the subpolar North Atlantic. However, we use the term "cold blob" as it more accurately reflects the statistically significant cooling trend observed over the subpolar North Atlantic, as discussed in detail in section 2a.

DOI: 10.1175/JCLI-D-23-0654.1

intertropical convergence zone (Karnauskas et al. 2021), the distribution of marine heatwaves (Ren and Liu 2021), and climate sensitivity (Mitevski et al. 2023).

Despite the broad implications of the North Atlantic cold blob, the mechanisms underpinning its formation remain a subject of debate. A prevailing hypothesis attributes the existence of the cold blob to a slowdown of the Atlantic meridional overturning circulation (AMOC; e.g., Rahmstorf et al. 2015; Caesar et al. 2018), a large-scale ocean circulation responsible for northward oceanic heat transport (OHT) in the Atlantic Ocean (Johns et al. 2011). On decadal and longer time scales, a weaker AMOC is associated with less northward OHT and colder subpolar North Atlantic SST (Delworth et al. 1993; Zhang 2008; Zhang et al. 2019). The AMOC is typically projected to decline throughout the twenty-first century (Weijer et al. 2020), probably due to increased freshwater fluxes into the subpolar North Atlantic associated with Arctic sea ice loss (Jahn and Holland 2013; Sévellec et al. 2017; Gervais et al. 2018; Liu et al. 2019), Greenland ice sheet melting (Golledge et al. 2019), or increased Arctic runoff (Nummelin et al. 2016). The projected AMOC weakening and resultant northward OHT decrease might be responsible for a lack of warming over the subpolar North Atlantic, as suggested by heat budget diagnosis (Menary and Wood 2018) and sensitivity experiments (Sévellec et al. 2017; Liu et al. 2020).

However, a scarcity of direct ocean observations and recent studies challenge the notion that the AMOC-associated OHT decrease is the sole mechanism for the North Atlantic cold blob. Neither observational nor proxy-based AMOC reconstructions agree on the changes in the AMOC and associated OHT convergence (OHTC) over the historical period (Moffa-Sánchez et al. 2019; Fu et al. 2020; Caesar et al. 2021; Kilbourne et al. 2022). Climate models also disagree on the sign of the AMOC trend over the historical period (Weijer et al. 2020). Moreover, changes in wind-driven gyre circulations (Keil et al. 2020), intensified heat loss from the ocean to the atmosphere due to a trend toward more positive phase of North Atlantic Oscillation (Fan et al. 2023), intensified surface wind (He et al. 2022), and more passage of midlatitude storms (Li et al. 2022) have all been suggested to play a role in driving the North Atlantic cold blob. Essentially, the subpolar North Atlantic SST variability on decadal and longer time scales can be influenced by multiple processes: OHT by overturning or gyre circulation (Bjerknes 1964; Zhang et al. 2019; Li et al. 2020); mixed layer depth variation (Yamamoto et al. 2020), stochastic atmosphere-induced surface heat flux forcing (Clement et al. 2015; Liu et al. 2023), ocean–atmosphere coupling (Delworth et al. 2017; Trossman et al. 2016; Small et al. 2020), and external radiative forcing such as anthropogenic aerosols and greenhouse gases (Booth et al. 2012; Bellomo et al. 2018) and volcanic eruption (Mann et al. 2021). The multifaceted nature of subpolar North Atlantic SST variability makes it challenging to identify the causes of historical SST trends.

This study uses abundant outputs from phase 6 of Coupled Model Intercomparison Project (CMIP6; Eyring et al. 2016) to examine the reproducibility of the North Atlantic cold blob within the current generation of climate models and assess the consensus among these models regarding the mechanisms driving the cold blob. Through the analysis, we aim to elucidate the mechanisms behind the North Atlantic cold blob and contribute to our understanding of model behaviors in representing the North Atlantic climate. The remainder of the manuscript is as follows. Section 2 introduces data and an SST trend decomposition framework we use to diagnose the cold blob formation mechanism. In section 3, we evaluate model performance in simulating the North Atlantic cold blob and analyze the underlying mechanisms for the simulated North Atlantic cold blob. We find that the models highly spread in the predominant process driving the cold blob and further explore the potential factors causing the model spread in section 4. We present our conclusions and highlight the implications of our findings in section 5.

2. Data and methods

a. *Observation-based SST datasets*

To quantify the centennial trend of SST anomalies over the subpolar North Atlantic, three observational SST estimates are used, namely, the 1° × 1° HadISST (Rayner et al. 2003), the 2° × 2° ERSST, version 5 (Huang et al. 2017), and the 5° × 5° Kaplan Extended SST version 2 (Reynolds and Smith 1994). Despite slight differences in the location, spatial extent, and magnitude of the cooling, all three datasets show cooling SSTs over 1900–2014 to the southeast of Greenland and over the Irminger Sea (cyan boxes in Fig. 1). On account of the agreement among the three datasets, we use their average as the best estimate of the subpolar North Atlantic SST trend, which is further used to evaluate the performance of CMIP6 models in simulating cold blob over the twentieth century. According to the dataset average, the SST over the Irminger Sea is cooling at a rate of 0.19 K century^{-1} (90% confidence interval of the linear trend: [−0.40, 0.00]). It is noteworthy that the SST trend over the subpolar North Atlantic is subject to climate variability on decadal and longer time scales (Delworth and Mann 2000; Delworth et al. 2016; Robson et al. 2018; Zhang et al. 2019). Nevertheless, the three observational SST datasets consistently show a region of statistically significant cooling over the subpolar North Atlantic. Thus, in this study, we call the pattern of subpolar North Atlantic SST change the "cold blob" rather than the "warming hole," which refers to a muted or lack of warming in the region, as in many other studies (Drijfhout et al. 2012; Rahmstorf et al. 2015; Menary and Wood 2018; Gervais et al. 2018).

b. *CMIP6 models*

A total of 32 models, which output SST (model variable named as "tos"), overturning streamfunction, and variables needed for heat budget analysis (see section 2c for details) under the historical all-forcing simulations, are analyzed to assess their performance of reproducing the observed North Atlantic cold blob (Table S1 in the online supplemental material). For models with multiple realizations, results are averaged over ensemble members, if not specifically noted. Linear trends of annual-mean SSTs are calculated over 1900–2014 to quantify the centennial

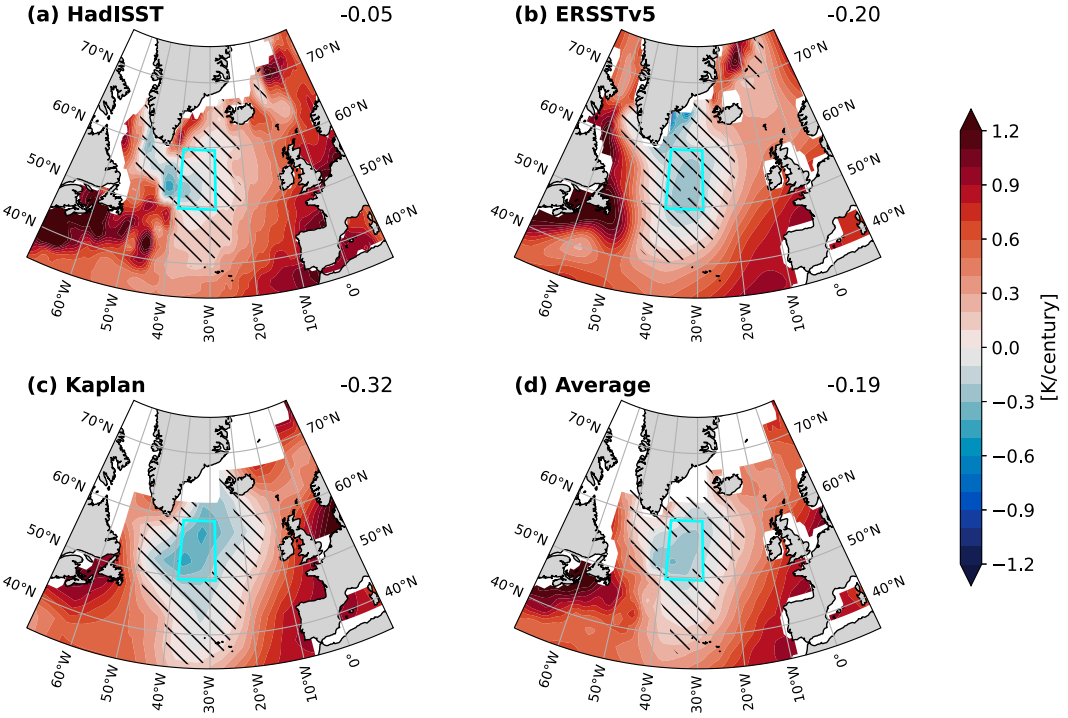

FIG. 1. Linear trends of annual-mean SSTs over 1900–2014. Individual panels are for (a) HadISST, (b) ERSSTv5, (c) Kaplan SST, and (d) the average over (a)–(c). For HadISST, regions where sea ice exists are masked. The three observational datasets are interpolated onto 1° × 1° grids before averaging. Trends are calculated using ordinary least squares. In (a)–(c), hatches denote the region where the trend is statistically insignificant at the 90% confidence level according to the Student's *t* test; in (d), hatches denote the region where one dataset shows different signs of trend from the other two. The cyan boxes show the observed cold blob region, with respective regional mean trends (K century^{-1}) on the top right of individual panels.

changes in subpolar North Atlantic SST. The data are interpolated linearly into the same 1° × 1° grid cells before calculating the multimodel mean.

The AMOC is commonly defined as the zonally integrated northward volume transport, thus a function of latitude and depth with a unit of cubic meters per second (m^3 s^{-1}) or more commonly as Sverdrup (Sv; 1 Sv ≡ 10^6 m^3 s^{-1}) in physical oceanography. The direct model output variable, overturning mass streamfunction ("msftmz" or "msftyz"), corresponds to its common definition if multiplied by the seawater density (e.g., 1.03 × 10^9 kg s^{-1} = 1 Sv, assuming the seawater density is 1030 kg m^{-3}). The strength of the two-dimensional AMOC is represented by an AMOC index defined as the maximum overturning streamfunction within 10°–90°N, below the depth of 500 m. The maximum usually occurs at a latitude of around 35°N and a depth of 1000 m, although the specific location could somewhat vary across models. An alternative AMOC index is defined at a fixed latitude across all models. As our main conclusions remain unchanged with whichever definition is used (appendix B), we base our analysis on the first definition in this study.

c. *SST trend decomposition*

We use the partial temperature change (PTC) decomposition framework (Lu and Cai 2009) that decomposes the SST trend to individual radiative, surface, and oceanic processes based on ocean's energy budget to quantify the mechanism of cold blob formation. This method has been extensively used to study the mechanisms of SST changes, such as those over the Arctic (Lee et al. 2017) and the North Atlantic (Fan et al. 2021).

According to the energy budget of a local ocean column, the time rate of change in annual-mean ocean heat content (OHC = $\int_{-D}^{\eta} \rho C_P \theta dz$, where η is the sea surface height, D is the depth of seafloor, ρ is the seawater density, and θ is the potential temperature) is determined by the net downward heat flux at the surface Q and the divergence of horizontal ocean heat transport ($\mathbf{OHT} = \int_{-D}^{\eta} \rho C_P \mathbf{u}\theta dz$, where $\mathbf{u}$ is the velocity of ocean current):

$$\frac{\partial \mathrm{OHC}}{\partial t} = Q - \nabla \cdot \mathbf{OHT}. \tag{1}$$

Here, Q is the sum of surface radiative and heat fluxes, including the net shortwave (SW) radiation [$(1-\alpha)\mathrm{SW}^{\downarrow}$, where α is surface albedo], net longwave (LW) radiation ($\mathrm{LW}^{\downarrow} - \mathrm{LW}^{\uparrow}$), and sensible heat (SH) and latent heat (LH) fluxes. In appendix A, we compare the magnitude of individual terms in Eq. (1) and confirm that, on the time scale longer than 25 years, the magnitude of $\partial \mathrm{OHC}/\partial t$ is one magnitude smaller than Q in the cold blob region. Hence, Q has to be largely balanced by

$\nabla \cdot \mathbf{OHT}$ on multidecadal time scales. We therefore infer $-\nabla \cdot \mathbf{OHT}$, which we call OHTC, as the residual term of Q, i.e., $-\nabla \cdot \mathbf{OHT} \approx -Q$. The term Q has a full expression,

$$Q = (1 - \alpha)\mathrm{SW}^{\downarrow} + \mathrm{LW}^{\downarrow} - \mathrm{LW}^{\uparrow} - \mathrm{SH} - \mathrm{LH}. \quad (2)$$

Assuming seawater is a blackbody with emissivity equal to 1, the upward longwave radiation $\mathrm{LW}^{\uparrow}$ can be expressed as $\mathrm{LW}^{\uparrow} = \sigma T^4$, where σ is the Stefan–Boltzmann constant and T is the surface temperature in the unit of K. On account that cloud can influence both shortwave and longwave radiation, we further diagnose cloud radiative forcing (CRF) as the difference between full-sky and clear-sky conditions; i.e., $\mathrm{SW}^{\downarrow(\mathrm{CRF})} = \mathrm{SW}^{\downarrow} - \mathrm{SW}^{\downarrow(\mathrm{clear\text{-}sky})}$ and $\mathrm{LW}^{\downarrow(\mathrm{CRF})} = \mathrm{LW}^{\downarrow} - \mathrm{LW}^{\downarrow(\mathrm{clear\text{-}sky})}$. Substituting individual terms and taking the linear trend of Eq. (2) yields

$$\begin{aligned}\Delta Q \quad &= \Delta\{(1 - \alpha)[\mathrm{SW}^{\downarrow(\mathrm{CRF})} + \mathrm{SW}^{\downarrow(\mathrm{clear\text{-}sky})}]\} \\ &+ \Delta[\mathrm{LW}^{\downarrow(\mathrm{CRF})} + \mathrm{LW}^{\downarrow(\mathrm{clear\text{-}sky})}] \\ &- \Delta(\sigma T^4) - \Delta(\mathrm{SH} + \mathrm{LH}), \end{aligned} \quad (3)$$

where Δ denotes a linear operation of calculating trends.

Linearizing Eq. (3) around some basic state and neglecting higher-order terms, ΔQ becomes

$$\begin{aligned}\Delta Q = &-\Delta\alpha\overline{\mathrm{SW}^{\downarrow}} + (1 - \overline{\alpha})[\Delta\mathrm{SW}^{\downarrow(\mathrm{clear\text{-}sky})} + \Delta\mathrm{SW}^{\downarrow(\mathrm{CRF})}] \\ &+ \Delta\mathrm{LW}^{\downarrow(\mathrm{clear\text{-}sky})} + \Delta\mathrm{LW}^{\downarrow(\mathrm{CRF})} \\ &- \Delta(\mathrm{SH} + \mathrm{LH}) - 4\sigma\overline{T}^3\Delta T, \end{aligned} \quad (4)$$

where $\overline{(\cdot)}$ represents climatological values. Utilizing the balance between Q and $\nabla \cdot \mathbf{OHT}$ on multidecadal time scales, Eq. (4) becomes

$$\begin{aligned}\Delta(\nabla \cdot \mathbf{OHT}) = &-\Delta\alpha\overline{\mathrm{SW}^{\downarrow}} + (1 - \overline{\alpha})[\Delta\mathrm{SW}^{\downarrow(\mathrm{clear\text{-}sky})} \\ &+ \Delta\mathrm{SW}^{\downarrow(\mathrm{CRF})}] + \Delta\mathrm{LW}^{\downarrow(\mathrm{clear\text{-}sky})} \\ &+ \Delta\mathrm{LW}^{\downarrow(\mathrm{CRF})} - \Delta(\mathrm{SH} + \mathrm{LH}) - 4\sigma\overline{T}^3\Delta T, \end{aligned} \quad (5)$$

Dividing Eq. (5) by $4\sigma\overline{T}^3$ and rearranging terms lead to the PTC framework, which allows for quantifying surface temperature changes due to individual processes,

$$\Delta T = \frac{1}{4\sigma\overline{T}^3}\Bigg\{\underbrace{-\Delta\alpha\overline{\mathrm{SW}^{\downarrow}}}_{\text{T1: SAF}} + \overbrace{\underbrace{\Delta\mathrm{LW}^{\downarrow(\mathrm{CRF})}}_{\text{T2: LW CRF}} + \underbrace{\Delta\mathrm{SW}^{\downarrow(\mathrm{CRF})}}_{\text{T3: SW CRF}} + \underbrace{(1 - \overline{\alpha})[\Delta\mathrm{SW}^{\downarrow(\mathrm{clear\text{-}sky})}]}_{\text{T4: clear-sky SW}}}^{\text{Radiative}} + \underbrace{\Delta LW^{\downarrow(\mathrm{clear\text{-}sky})}}_{\text{T5: clear-sky LW}}$$

$$+ \underbrace{\Delta(-\nabla \cdot \mathbf{OHT})}_{\text{T6: OHTC}} \quad \underbrace{-\Delta(\mathrm{SH} + \mathrm{LH})}_{\text{T7: surface turbulent heat fluxes}}\Bigg\}. \quad (6)$$

The terms on the right-hand side of Eq. (6) are surface temperature trends decomposed into seven components associated with seven physical processes, which are, respectively, surface albedo feedback (SAF) (T1), longwave cloud radiative forcing (T2), shortwave cloud radiative forcing (T3), surface downward clear-sky shortwave radiation (T4), clear-sky longwave radiation (T5), OHTC (T6), and surface turbulent heat fluxes (T7). Note that all variables are directly output by models, except that we calculate surface albedo as $\alpha = \mathrm{SW}^{\uparrow}/\mathrm{SW}^{\downarrow}$. Comparing the sum of all PTC terms in Eq. (6) and simulated SST trends yields negligible differences in the extratropical North Atlantic, suggesting the validity of the PTC framework for diagnosing the mechanism of historical cold blob formation.

3. Results

a. North Atlantic cold blob simulated by CMIP6 models

The 32 CMIP6 models show considerable spread in the spatial pattern of 1900–2014 SST trends over the extratropical North Atlantic (Fig. 2). Fourteen models simulate warming over the subpolar North Atlantic, with nine of them (the four CESM2 models, the two EC-EARTH models, the two IPSL models, and one MRI-ESM2-0) even simulating enhanced warming, which is in stark contrast to observations. A total of 11 out of the 32 CMIP6 models simulate statistically significant cooling trends over the subpolar North Atlantic, i.e., a cold blob, and are referred to as "Cold Blob" models hereafter. As this study intends to understand the mechanism underlying the cold blob formation, we will focus on these Cold Blob models.

Among the 11 Cold Blob models, the magnitude and location of simulated North Atlantic cold blobs are highly spread. For example, the simulated maximum cooling trend over the subpolar North Atlantic ranges from about -3.0 K century^{-1} in the Community Integrated Earth System Model (CIESM) to about -0.6 K century^{-1} in MPI-ESM1-2-HR. Moreover, the cooling patch concentrates over the region on the east to the southern tip of Greenland (around 40°W) in the CMCC-CM2-SR5, FGOALS-f3-L, INM-CM4-8, MPI-ESM1-2-HR, and MPI-ESM1-2-LR, whereas it is in the western portion of the subpolar gyre and extends westward to the Labrador Sea in FGOALS-g3, GISS-E2-1-G, and GISS-E3-G. In addition, Seoul National University Atmosphere Model

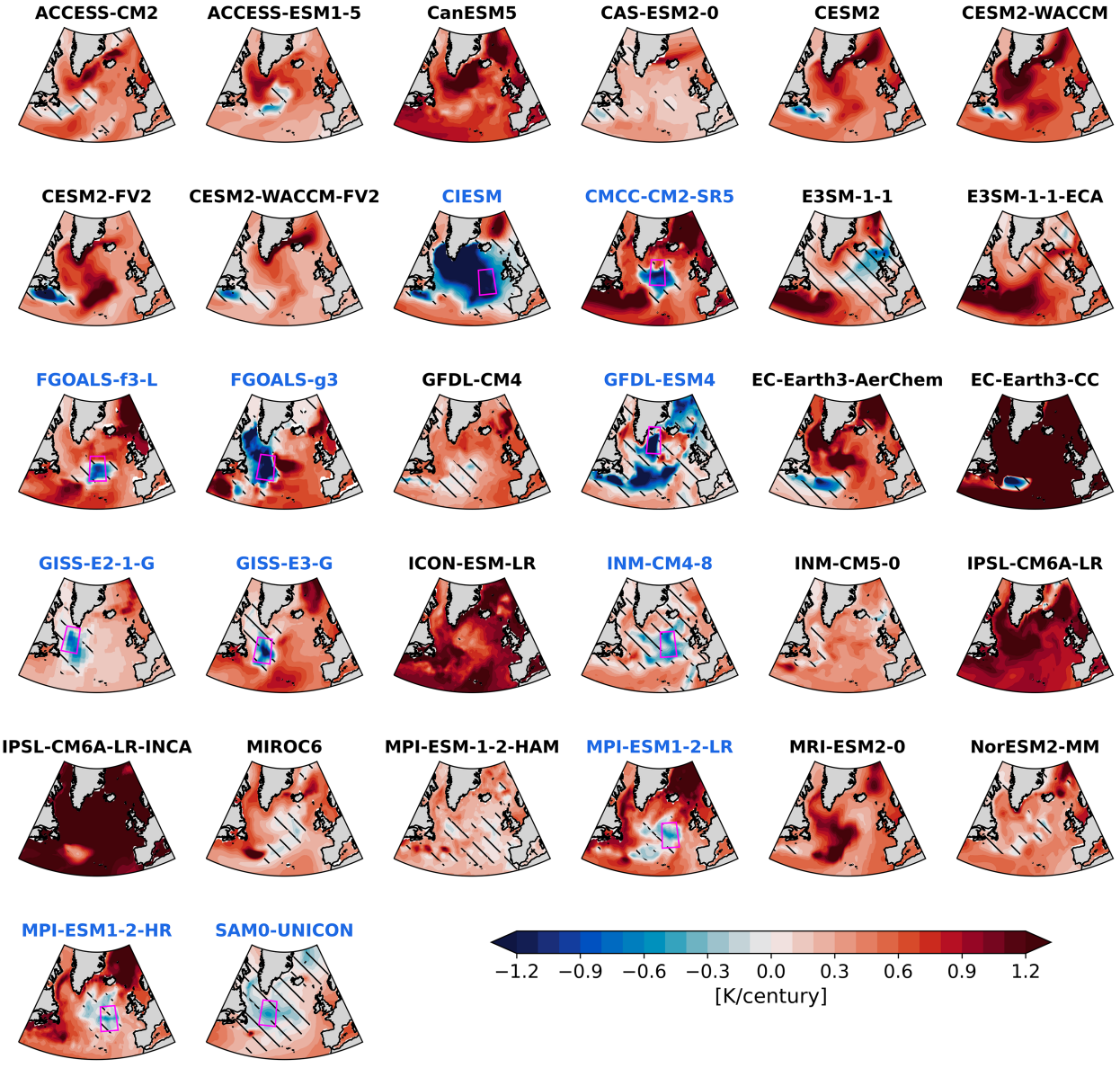

FIG. 2. Simulated 1900–2014 trends of ensemble-mean SST. Hatches denote statistically insignificant trends at the 90% confidence level. The magenta boxes denote the domain used to calculate the cold blob index in individual Cold Blob models, whose names are in blue.

Version 0 with a Unified Convection Scheme (SAM0-UNICON) simulates a cooling over most of the subpolar North Atlantic, which resembles the SST fingerprint of AMOC slowdown (Zhang 2008; Caesar et al. 2018), and CIESM simulates too strong a cooling over the entire midlatitude North Atlantic Ocean.

We also use a Taylor diagram (Fig. 3; Taylor 2001) to objectively evaluate how well a model reproduces the observed cold bold pattern. For each model, three statistics are examined, the pattern correlation between the simulated and observed SST trends (azimuthal angle), the ratio of the standard deviation of simulated SST trends across space between models and observations (distance to the origin), and the root-mean-square error normalized by observational standard error (distance to point [1, 0]). The pattern correlation ranges from −0.20 to 0.74. Notably, two models (CIESM and GFDL-ESM4), which simulate excessive cooling in the subpolar North Atlantic, show a negative pattern correlation with observations. Moreover, the spatial variability of the simulated SST trend is also spread among models. While five models simulate more than twice the magnitude of spatial variability compared to observations, three models show spatial variability less than half of the observed value. Among the 32 models, MPI-ESM1-2-HR overall performs the best in

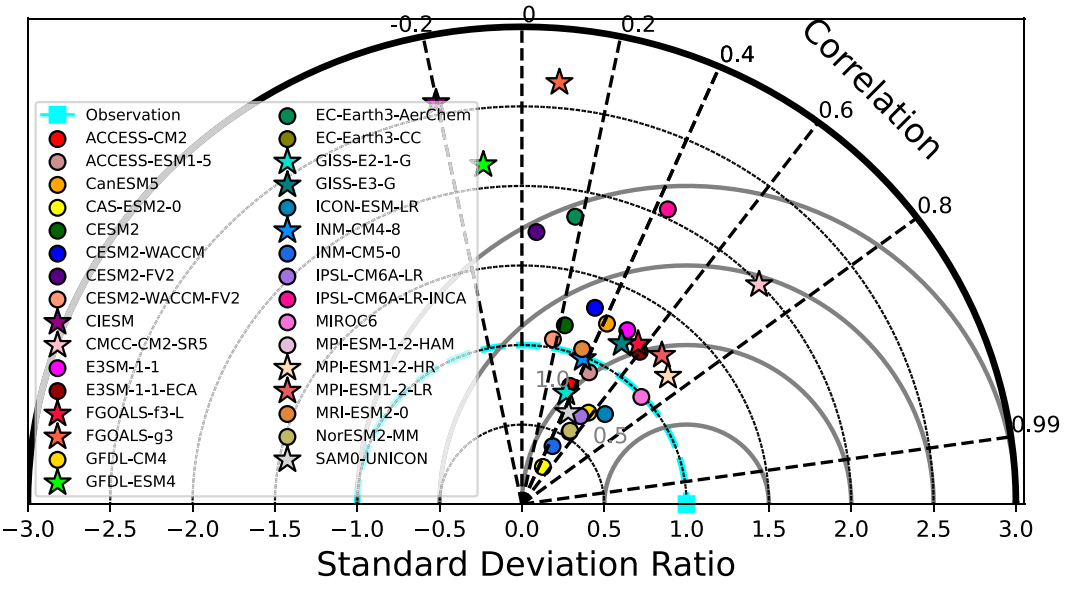

FIG. 3. Model–observation comparison of 1900–2014 SST trend pattern over the subpolar North Atlantic (40°–65°N, 10°–60°W). The observation is the average of three observational estimates. Stars denote the Cold Blob models.

capturing the observed SST trend pattern in the subpolar North Atlantic, showing the highest pattern correlation of 0.74 and a ratio of spatial standard deviation of 1.2.

Overall, CMIP6 models show highly spread skills in reproducing the observed pattern of subpolar North Atlantic SST trends throughout the twentieth century (Figs. 2 and 3). On account of this large spread, we proceed to examine the processes responsible for cold blob formation across the 11 Cold Blob models. We first define a cold blob index as the SST anomaly averaged over a 10° × 10° box centered on the location of minimum SST trend, which we call the "cold blob domain" (magenta boxes in Fig. 2). Note that this domain is model dependent. For example, the cold blob domain is 45°–55°N, 36°–46°W in FGOALS-g3, whereas it is 56°–66°N, 29°–39°W in GFDL-ESM4. Nevertheless, using a fixed cold blob domain, determined from observational SST trends, leads to qualitatively similar results (see appendix B for the robustness test). As expected, the cold blob index in the 11 models shows a decreasing trend from 1900 to 2014, ranging from −1.36 to −0.14 K century^{-1}, despite its decadal and multidecadal variability (Fig. 4).

b. *Physical processes contributing to the North Atlantic cold blob*

We apply the PTC framework [Eq. (6) in section 2c] to assess the mechanism of the centennial SST cooling in the Cold Blob models (Fig. 5). Among the seven PTC terms, surface albedo feedback (T1 in Fig. 5) plays a negligible role in the open ocean in all 11 Cold Blob models. Although albedo changes on sea ice margins (Bliss et al. 2019), such as those in the Labrador Sea, may have a contribution, their spatial pattern does not overlap with the cold blob region. The simulated cold blob formation, therefore, should be explained by the other six PTC terms (T2–T7). Among these terms, OHTC (T6) and surface turbulent heat fluxes (T7) are balanced on the first order; shortwave cloud radiative forcing (T2), longwave cloud radiative forcing (T3), surface downward clear-sky shortwave radiation (T4), and surface downward clear-sky shortwave radiation (T5) together balance the residual of the first-order terms (Figs. 5 and 6).

In each Cold Blob model, the decrease in OHTC (T6 in Fig. 5) has induced substantial cooling in the cold blob region, with a magnitude several times greater than the total cooling trend. However, the spatial pattern and the magnitude of the cooling vary with models. For example, OHTC-induced cooling spreads over the entire subpolar North Atlantic basin in CIESM, INM-CM4-8, MPI-ESM1-2-HR, MPI-ESM1-2-LR, and SAM0-UNICON, while it is confined to the western basin and the Labrador Sea in FGOALS-g3, GISS-E2-1-G, and GISS-E3-G and more localized regions in FGOALS-f3-L and GFDL-ESM4. Notably, the OHTC-associated cooling in SAM0-UNICON exhibits a typical pattern of AMOC's fingerprint suggested by previous studies (Zhang 2008): An SST anomaly dipole in the subpolar North Atlantic and the Labrador Sea and in the Gulf Stream extension region. The OHTC-induced cooling in GFDL-ESM4, however, occurs at higher latitudes, distinct from the typical AMOC fingerprint pattern. As OHTC is largely determined by ocean currents, the diversity in OHTC-induced SST trends may be associated with model simulation of the location and strength of the ocean currents, such as the AMOC. The potential effect of the base-state AMOC strength is discussed in detail in section 5.

The cooling induced by reduced OHTC is offset by changes in surface heat fluxes (T7), which show a similar pattern and magnitude but with an opposite sign (Fig. 5). Physically, variation of subpolar North Atlantic surface turbulent heat fluxes on multidecadal time scales is largely driven by oceanic processes and acts to damp the ocean-induced SST anomalies (Gulev et al. 2013;

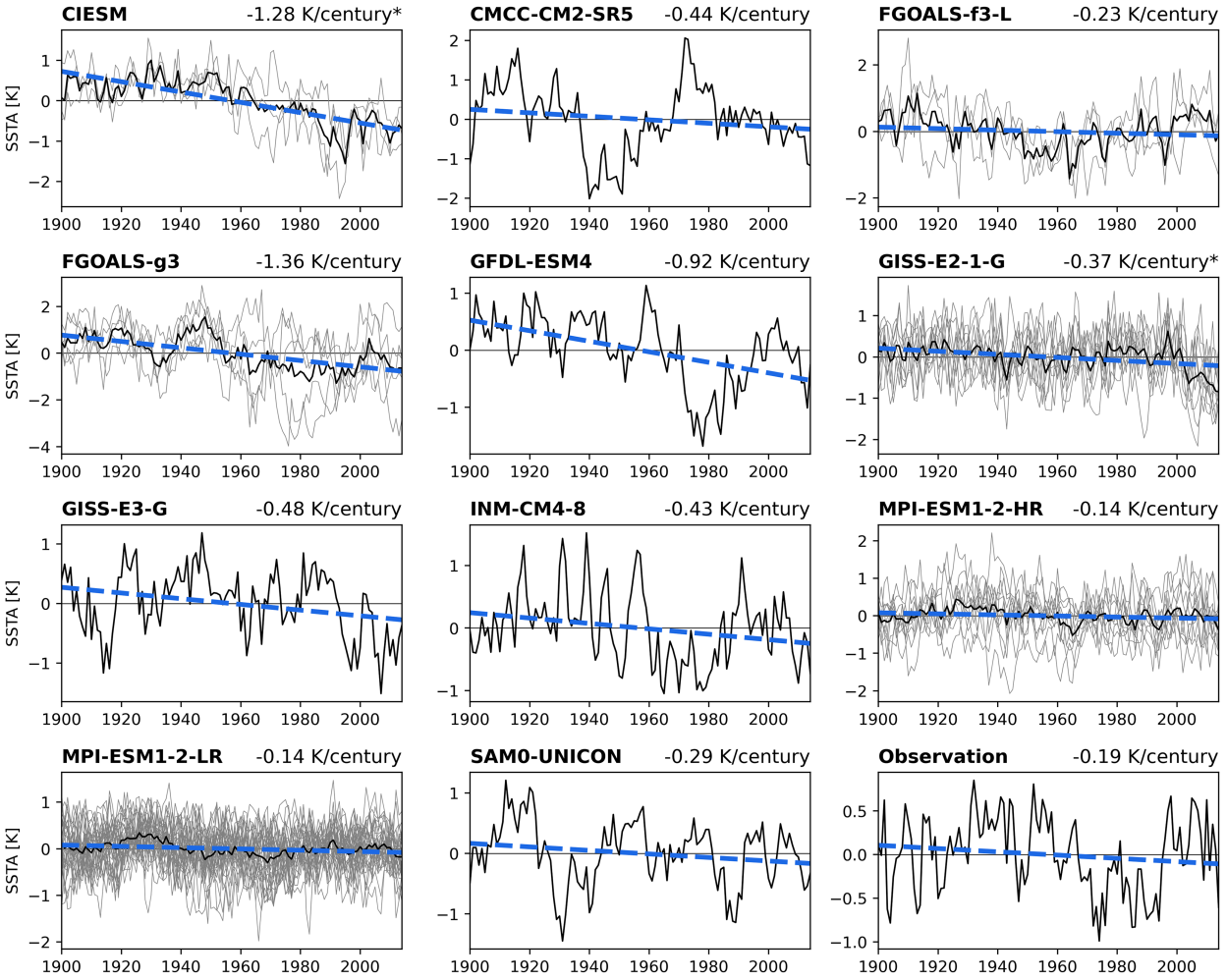

FIG. 4. Time series of simulated and observed cold blob index (K), calculated as the SST averaged over the boxes defined in Figs. 2 and 1d, respectively. For simulations, individual realizations are in gray thin lines, and the ensemble means are in thick black lines. Observation is the average over three observational SST estimates. In each panel, the dashed blue line denotes the linear trend of the back line, calculated using an ordinary least squares method. The value of the linear trend is shown on the top right of the panel, where * denotes statistical significance at the 90% confidence level after accounting for autocorrelations.

Zhang et al. 2016). For example, the surface turbulent heat flux from ocean to atmosphere reduces with a below-average SST through a thermodynamic adjustment of the marine atmospheric boundary layer to preexisting SST anomalies (Hausmann et al. 2017). On account of the physical association of T6 and T7, we combine the two terms in the discussion below and refer to the combined effect as "oceanic processes." The magnitude of the combined oceanic term is comparable to the simulated SST trend ("OHTC + SH&LH" in Fig. 6), yet its spatial pattern varies across models. For example, the oceanic process leads to warming concentrated in the eastern North Atlantic in MPI-ESM1-2-HR and MPI-ESM1-2-LR and warming in the entire North Atlantic basin (except the Irminger Sea) in GFDL-ESM4. Yet, it results in cooling in the western subpolar North Atlantic in the other eight models.

In addition, the four PTCs associated with radiative processes, namely, the "radiative" terms, explain a considerable portion of SST trends. First, cloud radiative forcing consistently shows perceptible contributions across models, but the magnitude and the spatial pattern of the associated SST trend exhibit a intermodel spread. The longwave cloud radiative forcing (T2 in Fig. 5) has decreased and led to cooling over most parts of the subpolar North Atlantic in all Cold Blob models, except in the western subpolar basin in FGOALS-g3 and the eastern subpolar basin in CIESM, CMCC-CM2-SR5, and GFDL-ESM4. In addition, the shortwave cloud radiative forcing (T3 in Fig. 5) has decreased and led to cooling over the entire basin in CIESM and GFDL-ESM4, the western basin in FGOALS-g3, and the eastern basin in CMCC-CM2-SR5, GISS-E3-G, MPI-ESM1-2-HR, MPI-ESM1-2-LR, and SAM0-UNICON but has increased and led to warming elsewhere. These intermodel differences might be associated with changes in multiple cloud properties, such as cloud type, cloud cover, and cloud-base height, which climate models could differ

FIG. 5. Partial temperature change terms [Eq. (6)] in the Cold Blob models. Shown from left to right are temperature changes due to SAF change (T1), LW CRF change (T2), SW CRF change (T3), non-SAF-induced change in clear-sky SW (T4), downwelling clear-sky LW radiation change (T5), OHTC change (T6), and surface turbulent heat flux change (T7). T1–T5 share the left color bar, and T6 and T7 share the right color bar.

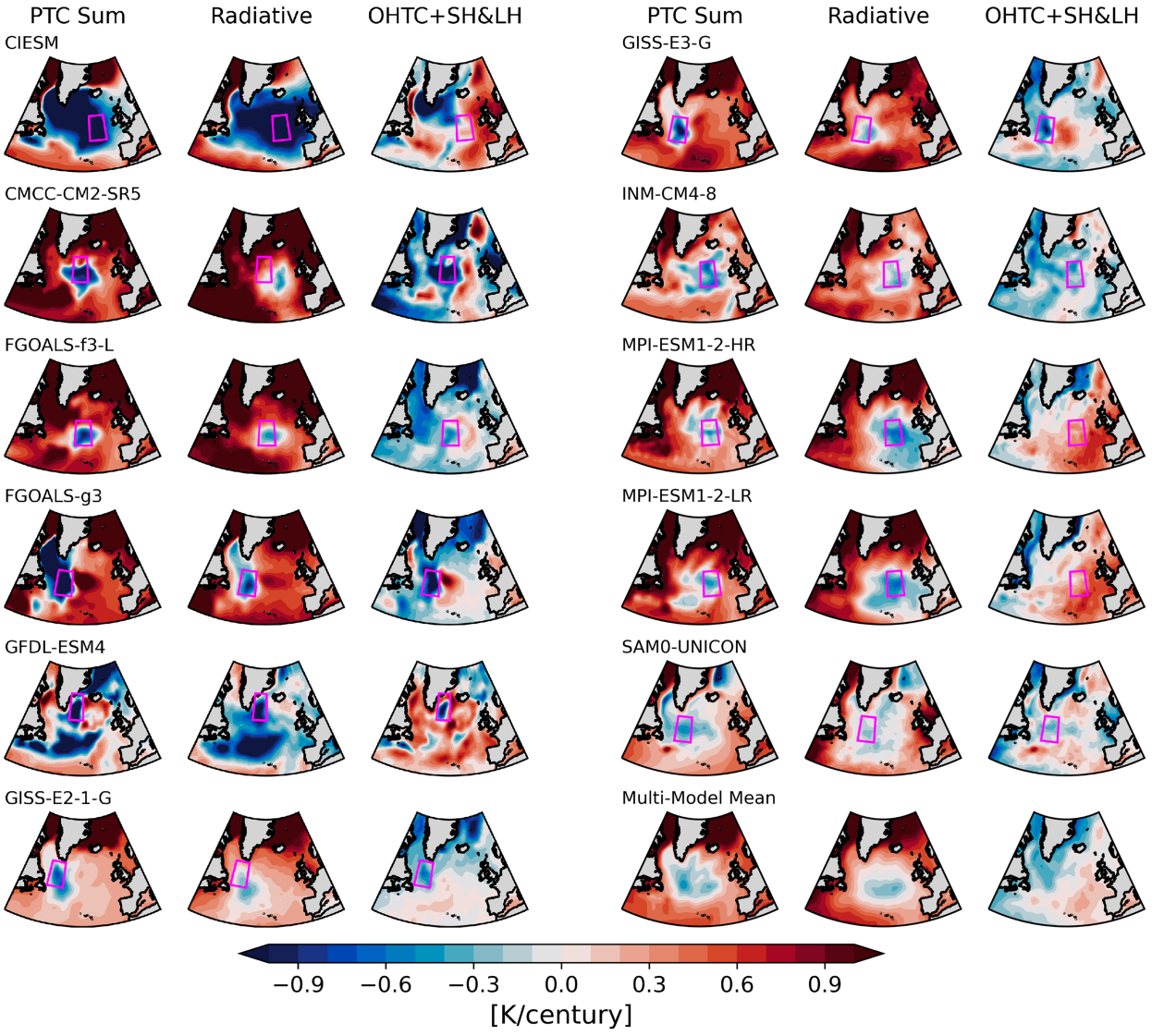

FIG. 6. (left) Sums of all PTCs, (middle) sums of PTCs associated with radiative processes (T2–T5), and (right) sums of PTCs due to changes in OHTC and surface heat fluxes (T6 and T7) in the 11 Cold Blob models and their multimodel mean.

significantly in representing (Ceppi et al. 2017). Second, the surface clear-sky downward SW, which is associated with the direct effect of aerosol forcing, shows a consistent decrease and resultant cooling across models, with a moderate intermodel spread in the magnitude of the cooling (T4 in Fig. 5). This intermodel spread in the direct aerosol radiative forcing is consistent with previous studies (Zhang et al. 2022).

Finally, changes in the surface clear-sky downward longwave flux (T5 in Fig. 5) lead to a lack of warming in most of the Cold Blob models, except in CIESM, FGOALS-f3-L, and GFDL-ESM4 where an absolute cooling is induced. These changes are a combination of changes in lower-troposphere temperature profiles and the concentration of atmospheric greenhouse gases, including water vapor. For instance, in GFDL-ESM4, despite the increase in greenhouse gases that efficiently emit longwave radiation, the cold blob present at the ocean surface might cool the lower troposphere through decreased turbulent heat flux from the ocean to the atmosphere such that the colder atmosphere radiates less longwave downward. Changes in these radiative processes jointly result in an SST cooling pattern that resembles the simulated cold blob, with minor differences between the sum of all PTCs and that of radiative terms (Fig. 6). For example, in CMCC-CM2-SR5, the cooling due to the radiative processes is smaller in both magnitude and spatial extent, compared to the simulated cold blob, whereas in MPI-ESM1-2-HR and MPI-ESM1-2-LR, the radiative terms lead to stronger cooling in a larger area than the simulated North Atlantic cold blob.

It is noteworthy that the substantial cooling induced by decreased OHTC (Fig. 6) and the net cooling effect due to radiative processes (Fig. 7) are consistently absent in models that simulate enhanced warming in the subpolar North Atlantic

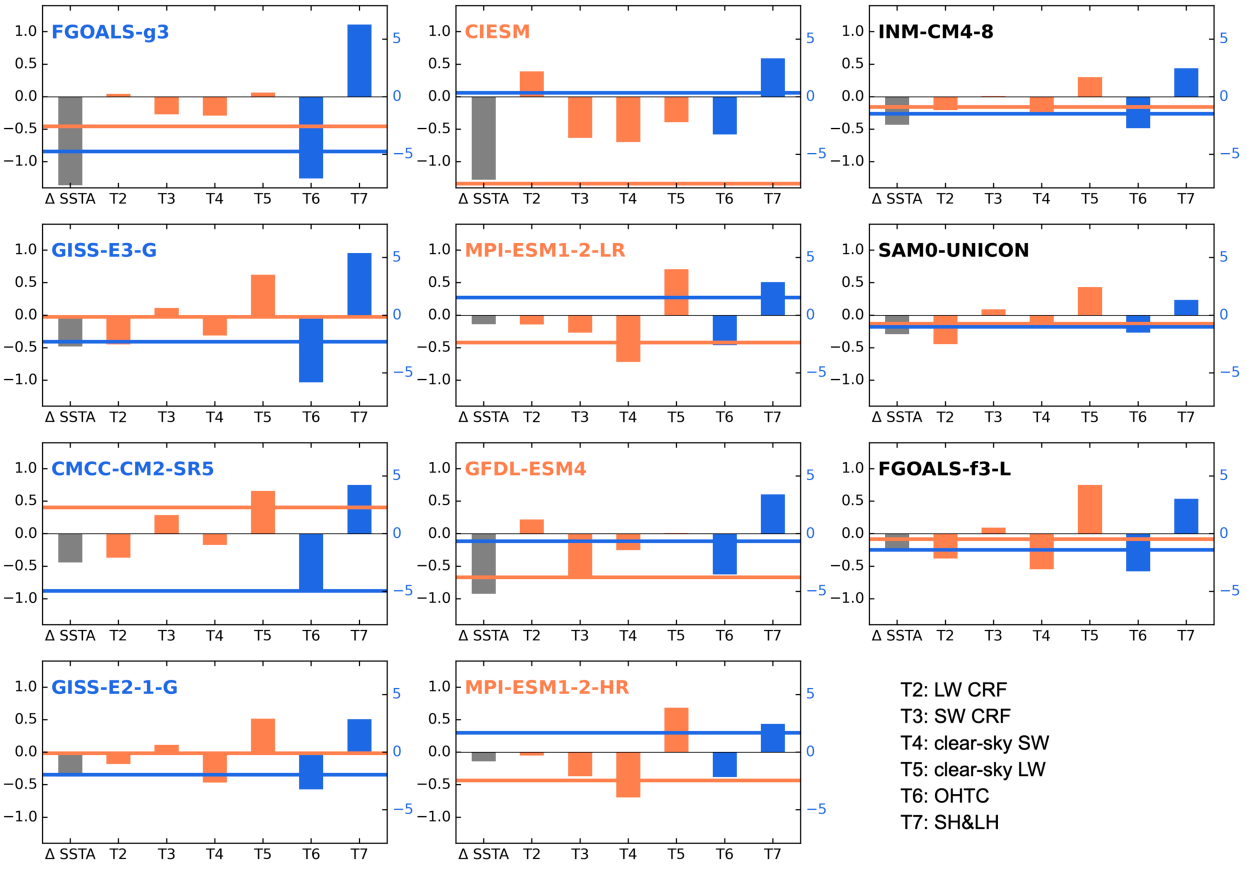

FIG. 7. SST trends and PTCs averaged within the respective cold blob region in each Cold Blob model (K century^{-1}). The SST trends and T2–T5 use the y axis on the left, and T6 and T7 use the one on the right. The orange line denote the sum of PTCs due to radiative processes (T2–T5; orange bars), and the blue line represents the sum of PTCs due to OHTC and surface turbulent heat fluxes (T6 and T7; blue bars). The four models where the cold blob predominantly results from radiative processes (Radiation Dominant models) have their name in orange, while those four with OHTC being the dominant contributor (OHTC Dominant models) in blue.

(see Figs. S1 and S2). The contrast between these models and the Cold Blob models underscores the critical roles of the OHTC decrease and the cooling effect from radiative processes in reproducing a North Atlantic cold blob within the CMIP6 models. Nevertheless, the prominence of either mechanism over the other varies across models, as evidenced by the differing magnitudes and spatial patterns of PTCs in the subpolar North Atlantic region (Figs. 5 and 6). The dominance of either the OHTC or the radiative processes may determine the final positioning of the induced North Atlantic cold blob. Specifically, the multimodel mean shows that the radiation-induced cooling is mostly in the eastern basin, while the net cooling effect from OHTC and surface turbulent heat fluxes tends to occur in the western basin and the Labrador Sea (Fig. 6). This positioning difference could be associated with the existence of significant ocean currents in the western basin and prevailing marine boundary layer cloud occurrence, along with distinctive aerosol sources, in the eastern basin (Jensen et al. 2021; Wang et al. 2022).

The model disagreement on the predominant cold blob mechanism can be further demonstrated from PTC terms averaged over the model-specific cold blob domain in each Cold Blob model (Fig. 7). In four models, the radiative processes provide the predominant cooling mechanism to the North Atlantic cold blob, with oceanic terms leading to a net warming (e.g., in MPI-ESM1-2-HR) or a negligible cooling (e.g., in GFDL-ESM4). In other words, the simulated cold blob primarily results from the imbalance between the radiative processes. We thus label these models, CIESM, GFDL-ESM4, MPI-ESM1-2-HR, and MPI-ESM1-2-LR, as "Radiation Dominant." These Radiation Dominant models on average simulate radiative processes' contribution to the cold blob as -0.72 K century^{-1} and other processes' contribution as 0.13 K century^{-1}. As a counterpart, another four models are labeled as "OHTC Dominant" as they simulate the cold blob as a result of the imbalance between the first-order processes—OHTC and surface turbulent heat fluxes. Specifically, they simulate the fourth greatest cooling effect of oceanic terms, which are -0.88, -0.84, -0.41, and -0.35 K per century by CMCC-CM2-SR5, FGOALS-g3, GISS-E3-G, and GISS-E2-1-G, respectively. In these OHTC Dominant models, radiative terms contribute to either net warming (e.g., CMCC-CM2-SR5) or relatively modest cooling (e.g., FGOALS-g3). They on average simulate the net effect of OHTC and surface turbulent heat fluxes as -0.62 K century^{-1} and that of other

processes as -0.02 K century^{-1}. In the remaining models, radiative and oceanic processes make comparable contributions to the simulated cold blob, which, on average, are -0.19 and -0.34 K century^{-1}, respectively.

Overall, we conclude that there is no model agreement on the formation mechanism of the North Atlantic cold blob. The spread of the dominant North Atlantic cold blob formation mechanisms has motivated us to explore the factors that cause the differentiation of the importance of radiative processes versus oceanic processes. In the following section, we propose the model spread in the base-state AMOC strength as a potential explanation.

4. Discussion

a. *Potential causes of model spread in oceanic processes' contribution*

By transporting warm surface water northward from the tropics, the AMOC plays a major role in redistributing heat in the North Atlantic (Johns et al. 2011). The AMOC-associated OHT varies with latitudes, which reaches the maximum, about 1.18 PW, at 15°N, and is about 0.8 PW around 45°N (Trenberth and Fasullo 2017). Besides, the AMOC could impact the subpolar North Atlantic climate by coupling with the atmosphere via cloud radiative feedback (Trossman et al. 2016), atmospheric circulation such as the North Atlantic Oscillation (Delworth et al. 2016; Kim et al. 2023), and sea ice properties (Liu and Fedorov 2022; Deng and Dai 2022). Current climate models highly diverge in simulating the base-state AMOC and its variability (Jackson et al. 2020; Weijer et al. 2020; Lin et al. 2023). Along 26°N, the mean AMOC strength ranges from 9.6 to 23 Sv across CMIP6 models, with a large spread in the latitude and depth of the maximum AMOC (Weijer et al. 2020). This model spread in the base-state AMOC could be further translated into uncertainties in model projection of future climate change, such as the rate of the AMOC decline (Jackson et al. 2020; Lin et al. 2023) and the associated North Atlantic warming hole and the poleward shift of the midlatitude jet (Bellomo et al. 2021).

Given the AMOC's relevance to the North Atlantic climate in climate models, we composite the base-state AMOC (1900–2014 climatology) simulated by in the OHTC Dominant models and the Radiation Dominant models (Fig. 8). We find that the base-state AMOC differs between the two groups of models. Specifically, the maximum intensity of the base-state AMOC is 24 Sv, averaged across all 11 Cold Blob models (Fig. 8a), but is 27 and 20 Sv in OHTC Dominant models and Radiation Dominant models, respectively (Figs. 8b,c). Comparatively, the AMOC base state is about 7 Sv stronger at the depth of 1 km and the latitude of 35°N (where the maximum AMOC usually occurs) in the OHTC Dominant models than in the Radiation Dominant models (Fig. 8d). This stark contrast suggests that the base-state AMOC could be a differentiator between the two predominant North Atlantic cold blob mechanisms among the two groups of the Cold Blob models. Across the Cold Blob models, the base-state AMOC intensity explains approximately 40% of the spread in the OHTC-induced cooling

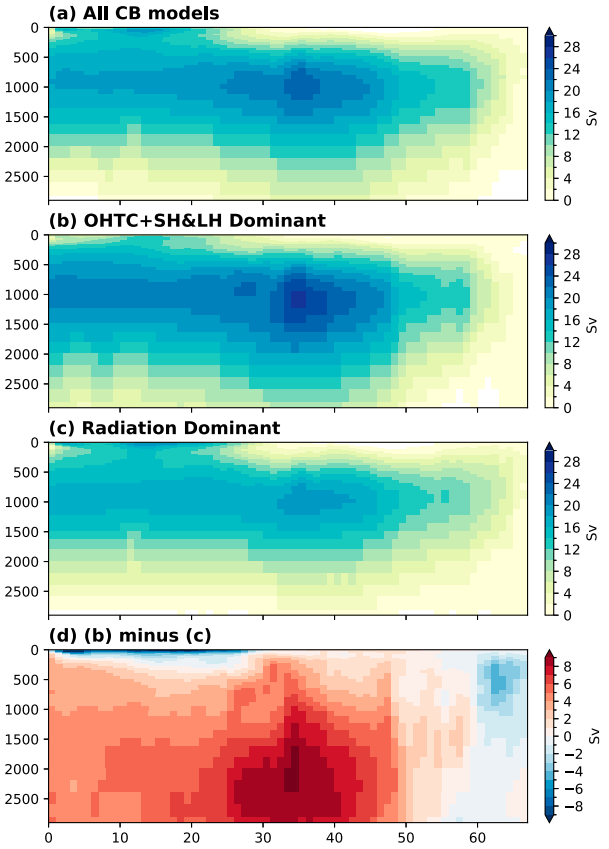

FIG. 8. The 1900–2014 climatology of the two-dimensional AMOC (Sv) averaged over (a) all Cold Blob models, (b) OHTC Dominant models, and (c) Radiation Dominant models. (d) The difference between (b) and (c).

(Fig. 9a). Taking into account surface turbulent flux's damping effect, the explained variance decreases to 25%, implying that the damping mechanism introduces uncertainty to the base-state AMOC's influence on the contribution of oceanic terms to the North Atlantic cold blob.

As a weakening AMOC is hypothesized to induce the North Atlantic cold blob or warming hole by decreasing OHT into the subpolar region (Rahmstorf et al. 2015; Keil et al. 2020; Liu et al. 2020), we quantify the contributions of AMOC-associated OHTC to the SST trend in each model and their dependence upon the AMOC base state. The effect of the AMOC intensity (denoted by ϕ and defined as the maximum AMOC north of 10°N and below 500 m) on the SST is commonly estimated as $\partial T/\partial\phi$ through linear regression. The AMOC could modulate subpolar North Atlantic SST not only through OHTC but also through other processes such as cloud radiative forcing (Trossman et al. 2016). Therefore, we quantify the sensitivity of SST to AMOC-associated OHTC as $S = (\partial T/\partial \mathrm{OHTC})(\partial \mathrm{OHTC}/\partial\phi)$. The effect of AMOC-associated OHTC on the SST trend hence can be mathematically written as $\Delta T_{\mathrm{OHTC},\phi} = (\partial T/\partial \mathrm{OHTC})(\partial \mathrm{OHTC}/\partial\phi)\Delta\phi$. Thus, the spreads in S and/or $\Delta\phi$ across models are expected to lead to the spread in $\Delta T_{\mathrm{OHTC},\phi}$. Further decomposition of S and $\Delta\phi$

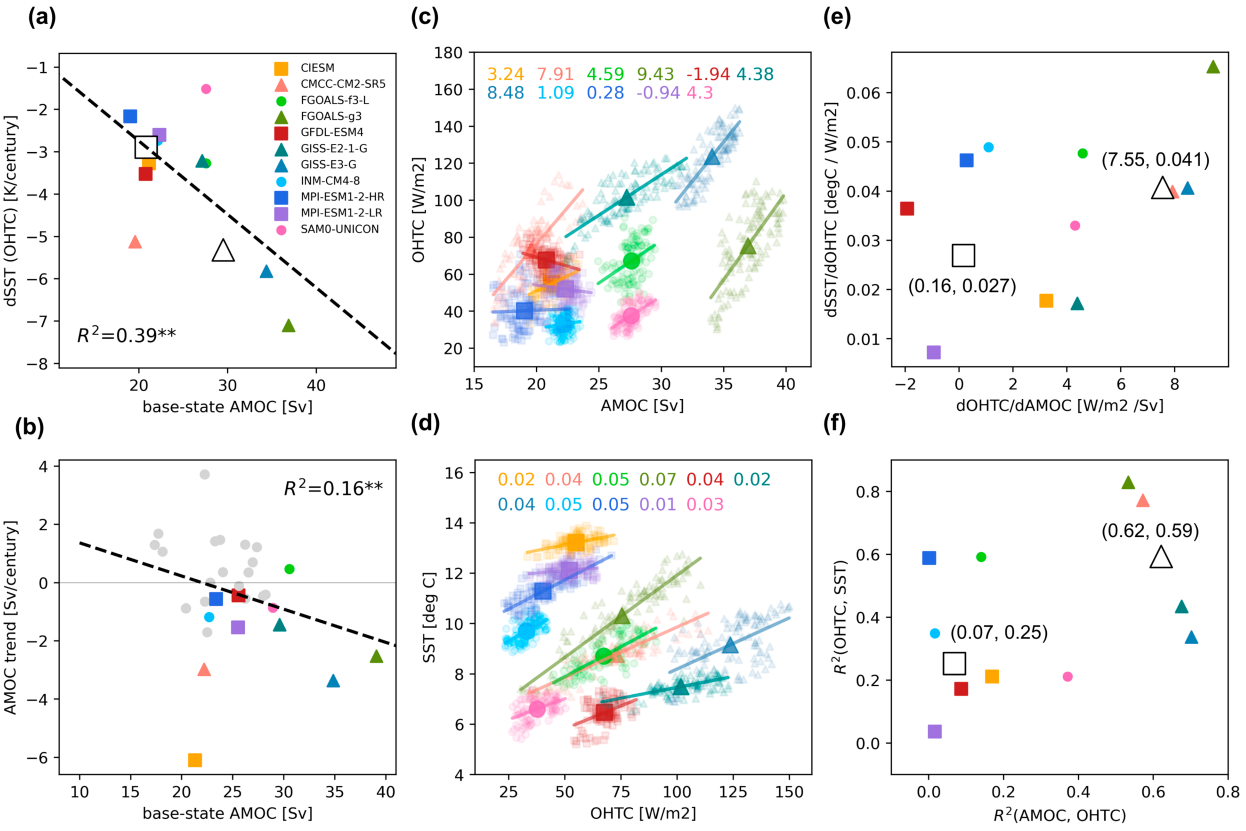

FIG. 9. (a) AMOC climatologies versus OHTC-induced SST changes in the cold blob region. Here, the AMOC strength is defined as the maximum overturning streamfunction north of 10°N and below 500 m in the Atlantic basin. (b) Climatologies and centennial trends of the AMOC simulated by all 32 CMIP6 models. The dashed line in (a) and (b) represents the linear regression between the two variables, and the corresponding explained variance R^2 is shown on the top right (** denotes statistical significance at a 95% confidence level). Note that the Cold Blob models are in color, while others in gray. The Radiation Dominant models, the OHTC Dominant models, and the rest of the Cold Blob models are marked by squares, triangles, and dots, respectively. The hollow square and triangle in (a) denote the average values over the Radiation Dominant models and OHTC Dominant models, respectively. (c) The relationship between detrended, 9-yr smoothed AMOC index, and domain-averaged OHTC in each Cold Blob model. Small transparent scatters show annual values, and large solid scatters represent 1900–2014 climatologies. Solid lines denote the linear regression in each model, with corresponding slope values noted on the top. (d) As in (c), but between detrended, 9-yr smoothed Cold Blob regional averages of OHTC and SST. Note that when estimating the relationship between the OHTC, the AMOC, and the SST, we only use one realization (r1i1p1f1) for the models that have multiple realizations available, as analogous to the real-world climate that has internal variability. (e) Sensitivity of OHTC to AMOC (x axis) versus sensitivity of SST to OHTC (y axis), estimated by the slope of regression shown in (c) and (d), respectively. The values denoted beside the triangle and the square are the average x-axis and y-axis values for OHTC Dominant and Radiation Dominant models. (f) As in (e), but for R^2 of the regression.

into the multimodel mean plus the difference from the mean leads to Eq. (7):

$$\Delta T^d_{\mathrm{OHTC},\phi} = S^m(\Delta\phi)^d + S^d(\Delta\phi)^m. \tag{7}$$

In Eq. (7), superscripts m and d, respectively, denote the multimodel mean and the difference from the mean. According to Eq. (7), we show that both $(\Delta\phi)^d$ and S^d are dependent on the base-state AMOC, with stronger AMOC accompanied by more significant AMOC slowdown in the past century and a larger sensitivity of SST to AMOC anomaly (Figs. 9b–f). Specifically, the base-state AMOC strength explains 16% of the spread in the historical AMOC change $[(\Delta\phi)^d]$ across the 32 CMIP6 models examined (Fig. 9b). Among them, the OHTC Dominant (Radiation Dominant) models on average show a base-state AMOC intensity of 29.4 (20.8) Sv and an AMOC decline of 2.6 (2.1) Sv century^{-1}. In other words, the OHTC Dominant models that simulate a stronger AMOC base state also simulate a 20% greater slowdown of the AMOC in the past century compared to their Radiation Dominant counterparts. Our findings here are consistent with previous studies reporting the base-state dependence of AMOC change under future forcing scenarios, even though the physical mechanisms behind remain an open question (Jackson et al. 2020; Lin et al. 2023).

Besides, the base-state AMOC can also affect the response of SST anomalies to AMOC anomaly S. Figures 9c–f illustrate the relationship between S and ϕ. Overall, the magnitude of

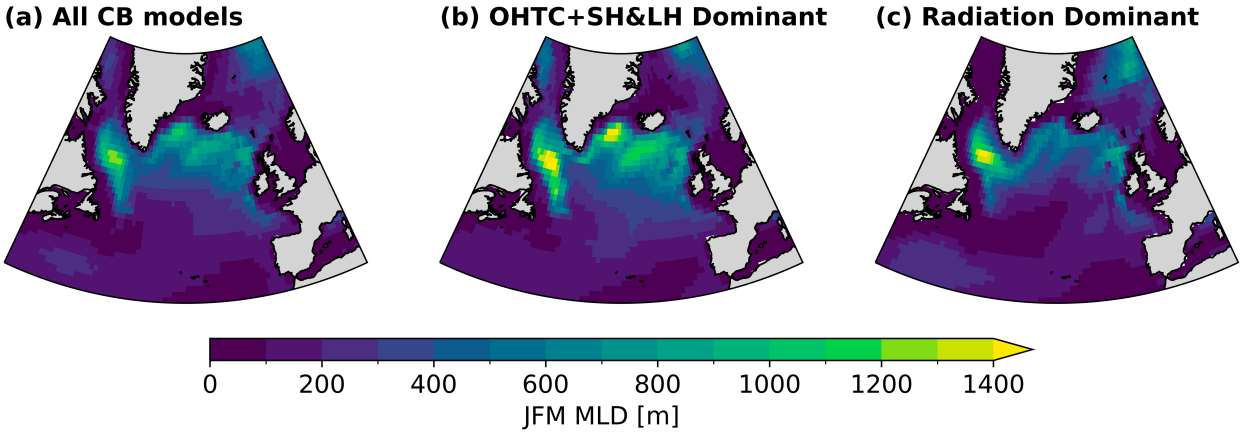

FIG. 10. January–March mean MLD (m) averaged over (a) all Cold Blob models, (b) OHTC Dominant models, and (c) Radiation Dominant models. CIESM, INM-CM4-8, and SAM0-UNICON do not have available MLD output, so that they are excluded from calculating the model composites.

S is greater in models with a stronger ϕ, indicating a stronger AMOC tends to play a more important role in modulating the OHTC and the SST variability in the subpolar North Atlantic. Mathematically, S is the product of two components: The sensitivity of OHTC within the Cold Blob region to the AMOC anomaly ($\partial\text{OHTC}/\partial\phi$) and the sensitivity of the SST to the OHTC anomaly ($\partial T/\partial\text{OHTC}$). We estimate the sensitivity, $\partial\text{OHTC}/\partial\phi$ and $\partial T/\partial\text{OHTC}$, as the slopes of linear regression of OHTC on AMOC and of SST on OHTC, as shown in Figs. 9c and 9d, respectively. The two sensitivity components for each Cold Blob model are summarized in Fig. 9e, and the corresponding explained variances are shown in Fig. 9f. First, in the Radiation Dominant models, the AMOC on average explains only 7% of the decadal OHTC variability (Fig. 9f; R^2 ranges from 0 to 0.17). This explained variance increases to 0.62 [0.53, 0.70] in the OHTC Dominant models, whose base-state AMOC is stronger by 8 Sv on average. Meanwhile, 1 Sv AMOC anomaly is on average associated with 7.55 W m^{-2} of OHTC anomaly in OHTC Dominant models, an order of magnitude larger than that in Radiation Dominant models (0.16 W m^{-2}). Second, in OHTC Dominant models, OHTC variability on average can explain 59% of the total SST variance on decadal time scales, which is more than twice the value for Radiation Dominant models (Fig. 9f). While 1 W m^{-2} of OHTC anomaly might on average induce a 0.041 K-SST anomaly in OHTC Dominant models, it is only associated with a 0.027-K SST anomaly in Radiation Dominant models (Fig. 9e). These intergroup differences suggest that the AMOC and the associated OHTC are more important to low-frequency SST variability in the subpolar North Atlantic when the base-state AMOC is relatively strong.

AMOC strength is closely linked to water mass transformation in the North Atlantic high latitudes (Isachsen et al. 2007; Grist et al. 2009; Langehaug et al. 2012), which allows the formation of North Atlantic Deep Water and the lower limb of the AMOC. Deep-water formation is often characterized by large mixed layer depth (MLD) that signifies the existence of deep convection, and it primarily occurs in regions like the Labrador Sea (Pickart and Spall 2007; Yashayaev and Loder 2017), the Irminger Sea and Iceland Basins (Lozier et al. 2019; Petit et al. 2020; Chafik et al. 2022), and the Nordic seas (Chafik and Rossby 2019). Current climate models show biases in representing deep-water formation in the North Atlantic (Heuzé 2017; Jackson and Petit 2023). Consistently, the Cold Blob models examined here also differ in simulating wintertime MLD in the deep-water formation regions (Fig. 10).

However, between the OHTC Dominant and Radiation Dominant models, the most significant discrepancy is over the Irminger Sea rather than the Labrador Sea, a location traditionally thought to be the most critical for deep-water formation and AMOC intensity. Specifically, the MLD in the Labrador Sea and the Irminger Sea reaches more than 1000 m in the OHTC Dominant models (Fig. 10b), while in the Radiation Dominant models, the MLD is approximately 1000 m in the Labrador Sea, similar to the OHTC dominant models, but reduces to 500 m in the Irminger Sea (Fig. 10c). The intergroup difference in the wintertime MLD climatology suggests that deep convection in the Irminger Sea, rather than the Labrador Sea, is more relevant to the intermodel spread in the base-state AMOC strength. The importance of the Irminger Sea deep convection shown in model simulations is consistent with the observational evidence suggesting that deep convection in the Irminger Sea and Iceland Basins, rather than the Labrador Sea, is largely responsible for the base-state AMOC (Lozier et al. 2019; Menary et al. 2020; Chafik et al. 2022).

It is worth mentioning that in addition to the MLD in deep-water formation regions, model spreads in representing the base-state AMOC can also be introduced by other factors such as the location of the North Atlantic Current (Jackson et al. 2020), the strength of the Nordic Sea overflow (Zhang et al. 2011), and model resolution (Roberts et al. 2020). Exploring these parameters in Cold Blob models and their contribution to the modeled base-state AMOC and long-term SST trend will be a valuable next step to address uncertainties in projecting subpolar North Atlantic climate change.

b. Model spread in radiative processes' contribution

Across the Cold Blob models, the oceanic process-induced SST change and the radiative process-induced SST change are

negatively correlated ($r = -0.54$); that is, models that simulate a greater-than-average cooling due to oceanic processes tend to simulate a smaller-than-average cooling due to radiative processes, especially cloud radiative forcing and clear-sky downward SW radiation. The base-state AMOC intensity, however, does not explain the model spread in radiative processes' contribution ($R^2 = 0.03$). Over 60% of the spread is from clear-sky downward longwave radiation-induced PTC, with 28% and 16% from PTCs due to clear-sky shortwave radiation and cloud radiative forcing, respectively. These processes indicate that the representation of feedback mechanisms, such as water vapor feedback and lapse rate feedback, in climate models might introduce uncertainties to radiative forcing on SST (Heinze et al. 2019). As examining these feedbacks is beyond the scope of this study, we leave it for future work.

5. Conclusions

Through an examination of CMIP6 historical simulations, we have found that the latest generation of climate models exhibits a considerable spread in simulating the century-long SST trend over the subpolar North Atlantic, with 11 out of 32 (34%) models simulating a cooling trend. These 11 so-called Cold Blob models, however, diverge in intensity, spatial coverage, and most importantly, the underlying mechanisms. Our analysis, utilizing the partial temperature change framework [Eq. (6)], indicates a divided understanding among the models: Four of the Cold Blob models simulate the imbalance between OHTC and surface turbulent heat flux as the primary mechanism, another four models simulate radiative processes as the key, and the two mechanisms play an equally important role in the remaining three models. Consequently, there is a notable lack of consensus regarding the mechanisms underlying the North Atlantic cold blob, leaving open the question of whether it can be attributed to a single process, such as an AMOC slowdown, gyre circulation change, or jet stream migration, as proposed by previous studies. Given the large uncertainties in identifying the mechanisms in simulations, single model-based studies on the North Atlantic cold blob should be interpreted with caution, especially when extrapolating to the geological past or future climate.

We further suggest that the intensity of the base-state AMOC might be a differentiator among models in terms of the predominant mechanisms driving the North Atlantic cold blob. On average, the base-state AMOC is about 7 Sv stronger in models with decreased OHTC as the predominant mechanism compared to those with radiative forcing as the primary driver for the simulated cold blob. Models' representation of the base-state AMOC might impact the simulated cold blob mechanism in two ways: a stronger AMOC tends to exert a more prominent influence on the ocean heat balance via OHTC and hence the SST variability over the subpolar North Atlantic; meanwhile, a stronger base-state AMOC is associated with a greater decrease in its strength in response to anthropogenic greenhouse gas forcing (Jackson et al. 2020; Lin et al. 2023), which may translate into a greater decrease in OHTC over the subpolar North Atlantic. As such, models with a stronger base-state AMOC tend to simulate a stronger cooling induced by the decrease in AMOC-associated OHTC.

We also found that the spread in base-state AMOC among the Cold Blob models is associated with wintertime MLD in the subpolar North Atlantic deep-water formation regions, in particular, the Irminger Sea. Deepened wintertime MLD reflects enhanced deep convection and water mass transformation, which strengthens the formation of North Atlantic Deep Water and the lower limb of the AMOC. The association between the base-state AMOC intensity and the Irminger Sea MLD is consistent with the latest observations suggesting that deep convection over the Irminger Sea is responsible for the mean-state AMOC in the subpolar North Atlantic (Lozier et al. 2019). Our results indicate that continued and focused monitoring of deep convection and overturning processes in the Irminger Sea is imperative. Such observational efforts are vital for refining climate models' representation of the base state of the AMOC, its variability, and the mechanisms driving long-term climate changes in the subpolar North Atlantic.

Acknowledgments. The authors thank the discussion with Drs. Susan Lozier, Eugene E. Clothiaux, Sukyoung Lee, Melissa Gervais, Raymond Najjar, and Chris Forest. YF and LL are supported by the National Aeronautics and Space Administration Grant 80NSSC22K0997 and the seed grant from the Institution of Computational and Data Sciences at the Pennsylvania State University. PZ is supported by the National Science Foundation, under Grant AGS 2232582.

Data availability statement. The Met Office HadISST1.1 dataset is available at https://www.metoffice.gov.uk/hadobs/hadisst/. The Kaplan Extended SST V2 and ERSST.v5 datasets are provided by the NOAA/OAR/ESRL PSL, Boulder, Colorado, United States, from their website at https://psl.noaa.gov. CMIP6 output can be accessed through the ESGF nodes (https://esgf-node.llnl.gov/search/cmip6/) and downloaded in Python environment using "acccmip6" (https://github.com/TaufiqHassan/acccmip6).

APPENDIX A

Ocean Heat Balance

It is a commonly used approach to estimate the ocean heat transport effect as a residual term from ocean heat balance (Xie et al. 2010; Roberts et al. 2017; Huguenin et al. 2022). In this study, we estimate ocean heat transport convergence $-\boldsymbol{\nabla} \cdot \mathbf{OHT}$ as a residual term in Eq. (6). It provides a convenient way to infer SST change due to OHTC without an explicit calculation from ocean currents and potential temperature, which itself causes heat budget disclosure due to discretization in time and space. We further assume that on multidecadal time scales, the time rate of change in ocean heat content ($\partial \mathrm{OHC}/\partial t$) is negligible. To examine to what extent $\partial \mathrm{OHC}/\partial t$ approximates to zero, we estimated OHC as $C_p \rho_0 \sum_i \theta(i) \delta z(i)$, where $C_p = 3900\ \mathrm{J\ kg^{-1}\ K^{-1}}$, $\rho_0 = 1026\ \mathrm{kg\ m^{-3}}$, $\theta(i)$ is the ocean potential temperature at the ith level, and $\delta z(i)$ is the interval distance between the ith level and the $(i + 1)$th level. We then smoothed the derived $\partial \mathrm{OHC}/\partial t$ and the net surface downward heat flux Q using a 25-yr moving window

and calculated the regional averages over the identified cold blob region specific to each model. Across the models examined, the ratio of $|\partial \mathrm{OHC}/\partial t|$ to $|Q|$ has a mean of 0.075 and a median of 0.052. Eight out of ten models show an average ratio of less than 0.1 (Fig. S3). Overall, $|\partial \mathrm{OHC}/\partial t|$ is at least one order smaller than $|Q|$, and Q largely balances with OHTC on the time scale of our interest. Thus, it is valid to use changes in the net surface downward heat flux ΔQ to approximate changes in the ocean heat transport effect on SST.

APPENDIX B

Robustness Test

We have tested the robustness of our results and conclusions against the choices of the cold blob domain, the time period for analysis, and the definition of the AMOC index. As mentioned in section 3a, aside from a fixed-sized cold blob domain, a variable-sized domain that includes all grid cells within the subpolar North Atlantic that show a decreasing trend of SST is used to calculate regional averages. We also conduct the same analysis for the period of 1900–89, which yields a stronger cooling trend of observational SST and a different group of Cold Blob models. Model grouping and key statistics using the second definition of cold blob domains or the 1900–89 period are summarized in Tables S1 and S2. With the use of a variable-sized cold blob domain, the variance of oceanic process-induced SST trend explained by the base-state AMOC decreases to 0.18. During the 1900–89 period, the observed North Atlantic cold blob magnitude is three times as large as that during the 1900–2014 period, and more CMIP6 models are qualified as Cold Blob models. Before the 1990s, most models simulate radiative processes as the predominant cooling mechanism, with seven models grouped as Radiation Dominant and only one model, CMCC-CM2-SR5, grouped as OHTC Dominant. However, the base-state AMOC strength still explains 29% of the model spread in the oceanic processes' contribution to the simulated cooling. Our findings remain robust if we use an alternative definition of the AMOC index, which is the maximum overturning at a fixed latitude (e.g., 40°N) across all models. The results are consistent in that 1) the multimodel means of the overturning strength along 40°N in the Radiation Dominant and OHTC Dominant models are 18.4 and 26.2 Sv, respectively, with an intergroup difference of 7.8 Sv; and 2) the sensitivity of subpolar North Atlantic OHTC to AMOC and the sensitivity of SST to OHTC both show a clear separation between the Radiation Dominant and OHTC Dominant models (Fig. S4). This is consistent with previous studies suggesting the coherence of AMOC variability across latitudes on multidecadal or longer time scales (Gu et al. 2020). Overall, it is robust that OHTC Dominant models simulate a stronger base-state AMOC and that maximum base-state AMOC strength can explain a significant fraction of the model spread in the oceanic processes' contribution to the North Atlantic cold blob.

REFERENCES

Bellomo, K., L. N. Murphy, M. A. Cane, A. C. Clement, and L. M. Polvani, 2018: Historical forcings as main drivers of the Atlantic multidecadal variability in the CESM large ensemble. *Climate Dyn.*, **50**, 3687–3698, https://doi.org/10.1007/s00382-017-3834-3.

——, M. Angeloni, S. Corti, and J. von Hardenberg, 2021: Future climate change shaped by inter-model differences in Atlantic meridional overturning circulation response. *Nat. Commun.*, **12**, 3659, https://doi.org/10.1038/s41467-021-24015-w.

Bjerknes, J., 1964: Atlantic air-sea interaction. *Adv. Geophys.*, **10**, 1–82, https://doi.org/10.1016/S0065-2687(08)60005-9.

Bliss, A. C., M. Steele, G. Peng, W. N. Meier, and S. Dickinson, 2019: Regional variability of Arctic Sea ice seasonal change climate indicators from a passive microwave climate data record. *Environ. Res. Lett.*, **14**, 045003, https://doi.org/10.1088/1748-9326/aafb84.

Booth, B. B. B., N. J. Dunstone, P. R. Halloran, T. Andrews, and N. Bellouin, 2012: Aerosols implicated as a prime driver of twentieth-century North Atlantic climate variability. *Nature*, **484**, 228–232, https://doi.org/10.1038/nature10946.

Caesar, L., S. Rahmstorf, A. Robinson, G. Feulner, and V. Saba, 2018: Observed fingerprint of a weakening Atlantic Ocean overturning circulation. *Nature*, **556**, 191–196, https://doi.org/10.1038/s41586-018-0006-5.

——, G. D. McCarthy, D. J. R. Thornalley, N. Cahill, and S. Rahmstorf, 2021: Current Atlantic meridional overturning circulation weakest in last millennium. *Nat. Geosci.*, **14**, 118–120, https://doi.org/10.1038/s41561-021-00699-z.

Ceppi, P., F. Brient, M. D. Zelinka, and D. L. Hartmann, 2017: Cloud feedback mechanisms and their representation in global climate models. *Wiley Interdiscip. Rev.: Climate Change*, **8**, e465, https://doi.org/10.1002/wcc.465.

Chafik, L., and T. Rossby, 2019: Volume, heat, and freshwater divergences in the subpolar North Atlantic suggest the Nordic Seas as key to the state of the meridional overturning circulation. *Geophys. Res. Lett.*, **46**, 4799–4808, https://doi.org/10.1029/2019GL082110.

——, N. P. Holliday, S. Bacon, and T. Rossby, 2022: Irminger Sea is the center of action for subpolar AMOC variability. *Geophys. Res. Lett.*, **49**, e2022GL099133, https://doi.org/10.1029/2022GL099133.

Clement, A., K. Bellomo, L. N. Murphy, M. A. Cane, T. Mauritsen, G. Rädel, and B. Stevens, 2015: The Atlantic multidecadal oscillation without a role for ocean circulation. *Science*, **350**, 320–324, https://doi.org/10.1126/science.aab3980.

Delworth, T., S. Manabe, and R. J. Stouffer, 1993: Interdecadal variations of the thermohaline circulation in a coupled ocean-atmosphere model. *J. Climate*, **6**, 1993–2011, https://doi.org/10.1175/1520-0442(1993)006%3C1993:IVOTTC%3E2.0.CO;2.

Delworth, T. L., and M. E. Mann, 2000: Observed and simulated multidecadal variability in the Northern Hemisphere. *Climate Dyn.*, **16**, 661–676, https://doi.org/10.1007/s003820000075.

——, F. Zeng, G. A. Vecchi, X. Yang, L. Zhang, and R. Zhang, 2016: The North Atlantic Oscillation as a driver of rapid climate change in the Northern Hemisphere. *Nat. Geosci.*, **9**, 509–512, https://doi.org/10.1038/ngeo2738.

——, ——, L. Zhang, R. Zhang, G. A. Vecchi, and X. Yang, 2017: The central role of ocean dynamics in connecting the North Atlantic Oscillation to the extratropical component of the Atlantic multidecadal oscillation. *J. Climate*, **30**, 3789–3805, https://doi.org/10.1175/JCLI-D-16-0358.1.

Deng, J., and A. Dai, 2022: Sea ice–air interactions amplify multidecadal variability in the North Atlantic and Arctic region. *Nat. Commun.*, **13**, 2100, https://doi.org/10.1038/s41467-022-29810-7.

Drijfhout, S., G. J. van Oldenborgh, and A. Cimatoribus, 2012: Is a decline of AMOC causing the warming hole above the North Atlantic in observed and modeled warming patterns? *J. Climate*, **25**, 8373–8379, https://doi.org/10.1175/JCLI-D-12-00490.1.

Eyring, V., S. Bony, G. A. Meehl, C. A. Senior, B. Stevens, R. J. Stouffer, and K. E. Taylor, 2016: Overview of the Coupled Model Intercomparison Project Phase 6 (CMIP6) experimental design and organization. *Geosci. Model Dev.*, **9**, 1937–1958, https://doi.org/10.5194/gmd-9-1937-2016.

Fan, Y., J. Lu, and L. Li, 2021: Mechanism of the centennial subpolar North Atlantic cooling trend in the FGOALS-g2 historical simulation. *J. Geophys. Res. Oceans*, **126**, e2021JC017511, https://doi.org/10.1029/2021JC017511.

——, W. Liu, P. Zhang, R. Chen, and L. Li, 2023: North Atlantic Oscillation contributes to the subpolar North Atlantic cooling in the past century. *Climate Dyn.*, **61**, 5199–5215, https://doi.org/10.1007/s00382-023-06847-y.

Fu, Y., F. Li, J. Karstensen, and C. Wang, 2020: A stable Atlantic meridional overturning circulation in a changing North Atlantic Ocean since the 1990s. *Sci. Adv.*, **6**, eabc7836, https://doi.org/10.1126/sciadv.abc7836.

Gervais, M., J. Shaman, and Y. Kushnir, 2018: Mechanisms governing the development of the North Atlantic warming hole in the CESM-LE future climate simulations. *J. Climate*, **31**, 5927–5946, https://doi.org/10.1175/JCLI-D-17-0635.1.

——, ——, and ——, 2020: Impact of the North Atlantic warming hole on sensible weather. *J. Climate*, **33**, 4255–4271, https://doi.org/10.1175/JCLI-D-19-0636.1.

Golledge, N. R., E. D. Keller, N. Gomez, K. A. Naughten, J. Bernales, L. D. Trusel, and T. L. Edwards, 2019: Global environmental consequences of twenty-first-century ice-sheet melt. *Nature*, **566**, 65–72, https://doi.org/10.1038/s41586-019-0889-9.

Grist, J. P., R. Marsh, and S. A. Josey, 2009: On the relationship between the North Atlantic meridional overturning circulation and the surface-forced overturning streamfunction. *J. Climate*, **22**, 4989–5002, https://doi.org/10.1175/2009JCLI2574.1.

Gu, S., Z. Liu, and L. Wu, 2020: Time scale dependence of the meridional coherence of the Atlantic meridional overturning circulation. *J. Geophys. Res. Oceans*, **125**, e2019JC015838, https://doi.org/10.1029/2019JC015838.

Gulev, S. K., M. Latif, N. Keenlyside, W. Park, and K. P. Koltermann, 2013: North Atlantic Ocean control on surface heat flux on multidecadal timescales. *Nature*, **499**, 464–467, https://doi.org/10.1038/nature12268.

Haarsma, R. J., F. M. Selten, and S. S. Drijfhout, 2015: Decelerating Atlantic meridional overturning circulation main cause of future west European summer atmospheric circulation changes. *Environ. Res. Lett.*, **10**, 094007, https://doi.org/10.1088/1748-9326/10/9/094007.

Hausmann, U., A. Czaja, and J. Marshall, 2017: Mechanisms controlling the SST air-sea heat flux feedback and its dependence on spatial scale. *Climate Dyn.*, **48**, 1297–1307, https://doi.org/10.1007/s00382-016-3142-3.

He, C., A. C. Clement, M. A. Cane, L. N. Murphy, J. M. Klavans, and T. M. Fenske, 2022: A North Atlantic warming hole without ocean circulation. *Geophys. Res. Lett.*, **49**, e2022GL100420, https://doi.org/10.1029/2022GL100420.

Heinze, C., and Coauthors, 2019: ESD reviews: Climate feedbacks in the Earth system and prospects for their evaluation. *Earth Syst. Dyn.*, **10**, 379–452, https://doi.org/10.5194/esd-10-379-2019.

Heuzé, C., 2017: North Atlantic deep water formation and AMOC in CMIP5 models. *Ocean Sci.*, **13**, 609–622, https://doi.org/10.5194/os-13-609-2017.

Huang, B., and Coauthors, 2017: Extended Reconstructed Sea Surface Temperature, version 5 (ERSSTv5): Upgrades, validations, and intercomparisons. *J. Climate*, **30**, 8179–8205, https://doi.org/10.1175/JCLI-D-16-0836.1.

Huguenin, M. F., R. M. Holmes, and M. H. England, 2022: Drivers and distribution of global ocean heat uptake over the last half century. *Nat. Commun.*, **13**, 4921, https://doi.org/10.1038/s41467-022-32540-5.

Isachsen, P. E., C. Mauritzen, and H. Svendsen, 2007: Dense water formation in the Nordic Seas diagnosed from sea surface buoyancy fluxes. *Deep-Sea Res. I*, **54**, 22–41, https://doi.org/10.1016/j.dsr.2006.09.008.

Jackson, L. C., and T. Petit, 2023: North Atlantic overturning and water mass transformation in CMIP6 models. *Climate Dyn*, **60**, 2871–2891, https://doi.org/10.1007/s00382-022-06448-1.

——, and Coauthors, 2020: Impact of ocean resolution and mean state on the rate of AMOC weakening. *Climate Dyn.*, **55**, 1711–1732, https://doi.org/10.1007/s00382-020-05345-9.

Jahn, A., and M. M. Holland, 2013: Implications of Arctic sea ice changes for North Atlantic deep convection and the meridional overturning circulation in CCSM4-CMIP5 simulations. *Geophys. Res. Lett.*, **40**, 1206–1211, https://doi.org/10.1002/grl.50183.

Jensen, M. P., V. P. Ghate, D. Wang, D. K. Apoznanski, M. J. Bartholomew, S. E. Giangrande, K. L. Johnson, and M. M. Thieman, 2021: Contrasting characteristics of open-and closed-cellular stratocumulus cloud in the eastern North Atlantic. *Atmos. Chem. Phys.*, **21**, 14 557–14 571, https://doi.org/10.5194/acp-21-14557-2021.

Johns, W. E., and Coauthors, 2011: Continuous, array-based estimates of Atlantic Ocean heat transport at 26.5°N. *J. Climate*, **24**, 2429–2449, https://doi.org/10.1175/2010JCLI3997.1.

Karnauskas, K. B., L. Zhang, and D. J. Amaya, 2021: The atmospheric response to North Atlantic SST trends, 1870–2019. *Geophys. Res. Lett.*, **48**, e2020GL090677, https://doi.org/10.1029/2020GL090677.

Keil, P., T. Mauritsen, J. Jungclaus, C. Hedemann, D. Olonscheck, and R. Ghosh, 2020: Multiple drivers of the North Atlantic warming hole. *Nat. Climate Change*, **10**, 667–671, https://doi.org/10.1038/s41558-020-0819-8.

Kilbourne, K. H., and Coauthors, 2022: Atlantic circulation change still uncertain. *Nat. Geosci.*, **15**, 165–167, https://doi.org/10.1038/s41561-022-00896-4.

Kim, H., and S.-I. An, 2013: On the subarctic North Atlantic cooling due to global warming. *Theor. Appl. Climatol.*, **114**, 9–19, https://doi.org/10.1007/s00704-012-0805-9.

Kim, H.-J., S.-I. An, J.-H. Park, M.-K. Sung, D. Kim, Y. Choi, and J.-S. Kim, 2023: North Atlantic Oscillation impact on the Atlantic meridional overturning circulation shaped by the mean state. *npj Climate Atmos. Sci.*, **6**, 25, https://doi.org/10.1038/s41612-023-00354-x.

Langehaug, H. R., P. B. Rhines, T. Eldevik, J. Mignot, and K. Lohmann, 2012: Water mass transformation and the North Atlantic current in three multicentury climate model simulations. *J. Geophys. Res.*, **117**, C11001, https://doi.org/10.1029/2012JC008021.

Lee, S., T. Gong, S. B. Feldstein, J. A. Screen, and I. Simmonds, 2017: Revisiting the cause of the 1989–2009 Arctic surface warming using the surface energy budget: Downward infrared radiation dominates the surface fluxes. *Geophys. Res. Lett.*, **44**, 10 654–10 661, https://doi.org/10.1002/2017GL075375.

Li, L., M. S. Lozier, and M. W. Buckley, 2020: An investigation of the ocean's role in Atlantic multidecadal variability. *J. Climate*, **33**, 3019–3035, https://doi.org/10.1175/JCLI-D-19-0236.1.

——, ——, and F. Li, 2022: Century-long cooling trend in subpolar North Atlantic forced by atmosphere: An alternative explanation. *Climate Dyn.*, **58**, 2249–2267, https://doi.org/10.1007/s00382-021-06003-4.

Lin, Y.-J., B. E. J. Rose, and Y.-T. Hwang, 2023: Mean state AMOC affects AMOC weakening through subsurface warming in the Labrador Sea. *J. Climate*, **36**, 3895–3915, https://doi.org/10.1175/JCLI-D-22-0464.1.

Liu, G., Y.-O. Kwon, C. Frankignoul, and J. Lu, 2023: Understanding the drivers of Atlantic multidecadal variability using a stochastic model hierarchy. *J. Climate*, **36**, 1043–1058, https://doi.org/10.1175/JCLI-D-22-0309.1.

Liu, W., and A. Fedorov, 2022: Interaction between Arctic sea ice and the Atlantic meridional overturning circulation in a warming climate. *Climate Dyn.*, **58**, 1811–1827, https://doi.org/10.1007/s00382-021-05993-5.

——, ——, and F. Sévellec, 2019: The mechanisms of the Atlantic meridional overturning circulation slowdown induced by Arctic sea ice decline. *J. Climate*, **32**, 977–996, https://doi.org/10.1175/JCLI-D-18-0231.1.

——, A. V. Fedorov, S.-P. Xie, and S. Hu, 2020: Climate impacts of a weakened Atlantic meridional overturning circulation in a warming climate. *Sci. Adv.*, **6**, eaaz4876, https://doi.org/10.1126/sciadv.aaz4876.

Lozier, M. S., and Coauthors, 2019: A sea change in our view of overturning in the subpolar North Atlantic. *Science*, **363**, 516–521, https://doi.org/10.1126/science.aau6592.

Lu, J., and M. Cai, 2009: Seasonality of polar surface warming amplification in climate simulations. *Geophys. Res. Lett.*, **36**, L16704, https://doi.org/10.1029/2009GL040133.

Mann, M. E., B. A. Steinman, D. J. Brouillette, and S. K. Miller, 2021: Multidecadal climate oscillations during the past millennium driven by volcanic forcing. *Science*, **371**, 1014–1019, https://doi.org/10.1126/science.abc5810.

Marshall, J., J. R. Scott, K. C. Armour, J.-M. Campin, M. Kelley, and A. Romanou, 2015: The ocean's role in the transient response of climate to abrupt greenhouse gas forcing. *Climate Dyn.*, **44**, 2287–2299, https://doi.org/10.1007/s00382-014-2308-0.

Menary, M. B., and R. A. Wood, 2018: An anatomy of the projected North Atlantic warming hole in CMIP5 models. *Climate Dyn.*, **50**, 3063–3080, https://doi.org/10.1007/s00382-017-3793-8.

——, L. C. Jackson, and M. S. Lozier, 2020: Reconciling the relationship between the AMOC and Labrador Sea in OSNAP observations and climate models. *Geophys. Res. Lett.*, **47**, e2020GL089793, https://doi.org/10.1029/2020GL089793.

Mitevski, I., Y. Dong, L. M. Polvani, M. Rugenstein, and C. Orbe, 2023: Non-monotonic feedback dependence under abrupt CO_2 forcing due to a North Atlantic pattern effect. *Geophys. Res. Lett.*, **50**, e2023GL103617, https://doi.org/10.1029/2023GL103617.

Moffa-Sánchez, P., and Coauthors, 2019: Variability in the Northern North Atlantic and Arctic Oceans across the last two millennia: A review. *Paleoceanogr. Paleoclimatol.*, **34**, 1399–1436, https://doi.org/10.1029/2018PA003508.

Nummelin, A., M. Ilicak, C. Li, and L. H. Smedsrud, 2016: Consequences of future increased Arctic runoff on Arctic Ocean stratification, circulation, and sea ice cover. *J. Geophys. Res. Oceans*, **121**, 617–637, https://doi.org/10.1002/2015JC011156.

Petit, T., M. S. Lozier, S. A. Josey, and S. A. Cunningham, 2020: Atlantic deep water formation occurs primarily in the Iceland basin and Irminger Sea by local buoyancy forcing. *Geophys. Res. Lett.*, **47**, e2020GL091028, https://doi.org/10.1029/2020GL091028.

Pickart, R. S., and M. A. Spall, 2007: Impact of Labrador Sea convection on the North Atlantic meridional overturning circulation. *J. Phys. Oceanogr.*, **37**, 2207–2227, https://doi.org/10.1175/JPO3178.1.

Rahmstorf, S., J. E. Box, G. Feulner, M. E. Mann, A. Robinson, S. Rutherford, and E. J. Schaffernicht, 2015: Exceptional twentieth-century slowdown in Atlantic Ocean overturning circulation. *Nat. Climate Change*, **5**, 475–480, https://doi.org/10.1038/nclimate2554.

Rayner, N. A., D. E. Parker, E. B. Horton, C. K. Folland, L. V. Alexander, D. P. Rowell, E. C. Kent, and A. Kaplan, 2003: Global analyses of sea surface temperature, sea ice, and night marine air temperature since the late nineteenth century. *J. Geophys. Res.*, **108**, 4407, https://doi.org/10.1029/2002JD002670.

Ren, X., and W. Liu, 2021: The role of a weakened Atlantic meridional overturning circulation in modulating marine heatwaves in a warming climate. *Geophys. Res. Lett.*, **48**, e2021GL095941, https://doi.org/10.1029/2021GL095941.

Reynolds, R. W., and T. M. Smith, 1994: Improved global sea surface temperature analyses using optimum interpolation. *J. Climate*, **7**, 929–948, https://doi.org/10.1175/1520-0442(1994)007%3C0929:IGSSTA%3E2.0.CO;2.

Roberts, C. D., M. D. Palmer, R. P. Allan, D. G. Desbruyeres, P. Hyder, C. Liu, and D. Smith, 2017: Surface flux and ocean heat transport convergence contributions to seasonal and interannual variations of ocean heat content. *J. Geophys. Res. Oceans*, **122**, 726–744, https://doi.org/10.1002/2016JC012278.

Roberts, M. J., and Coauthors, 2020: Sensitivity of the Atlantic meridional overturning circulation to model resolution in CMIP6 HighResMIP simulations and implications for future changes. *J. Adv. Model. Earth Syst.*, **12**, e2019MS002014, https://doi.org/10.1029/2019MS002014.

Robson, J., I. Polo, D. L. R. Hodson, D. P. Stevens, and L. C. Shaffrey, 2018: Decadal prediction of the North Atlantic subpolar gyre in the HiGEM high-resolution climate model. *Climate Dyn.*, **50**, 921–937, https://doi.org/10.1007/s00382-017-3649-2.

Sévellec, F., A. V. Fedorov, and W. Liu, 2017: Arctic sea-ice decline weakens the Atlantic Meridional Overturning Circulation. *Nat. Climate Change*, **7**, 604–610, https://doi.org/10.1038/nclimate3353.

Small, R. J., F. O. Bryan, S. P. Bishop, S. Larson, and R. A. Tomas, 2020: What drives upper-ocean temperature variability in coupled climate models and observations? *J. Climate*, **33**, 577–596, https://doi.org/10.1175/JCLI-D-19-0295.1.

Taylor, K. E., 2001: Summarizing multiple aspects of model performance in a single diagram. *J. Geophys. Res.*, **106**, 7183–7192, https://doi.org/10.1029/2000JD900719.

Trenberth, K. E., and J. T. Fasullo, 2017: Atlantic meridional heat transports computed from balancing Earth's energy locally. *Geophys. Res. Lett.*, **44**, 1919–1927, https://doi.org/10.1002/2016GL072475.

Trossman, D. S., J. B. Palter, T. M. Merlis, Y. Huang, and Y. Xia, 2016: Large-scale ocean circulation-cloud interactions reduce

the pace of transient climate change. *Geophys. Res. Lett.*, **43**, 3935–3943, https://doi.org/10.1002/2016GL067931.

Wang, J., and Coauthors, 2022: Aerosol and Cloud Experiments in the Eastern North Atlantic (ACE-ENA). *Bull. Amer. Meteor. Soc.*, **103**, E619–E641, https://doi.org/10.1175/BAMS-D-19-0220.1.

Weijer, W., W. Cheng, O. A. Garuba, A. Hu, and B. T. Nadiga, 2020: CMIP6 models predict significant 21st century decline of the Atlantic meridional overturning circulation. *Geophys. Res. Lett.*, **47**, e2019GL086075, https://doi.org/10.1029/2019GL086075.

Winton, M., S. M. Griffies, B. L. Samuels, J. L. Sarmiento, and T. L. Frölicher, 2013: Connecting changing ocean circulation with changing climate. *J. Climate*, **26**, 2268–2278, https://doi.org/10.1175/JCLI-D-12-00296.1.

Woollings, T., J. M. Gregory, J. G. Pinto, M. Reyers, and D. J. Brayshaw, 2012: Response of the North Atlantic storm track to climate change shaped by ocean–atmosphere coupling. *Nat. Geosci.*, **5**, 313–317, https://doi.org/10.1038/ngeo1438.

Xie, S.-P., C. Deser, G. A. Vecchi, J. Ma, H. Teng, and A. T. Wittenberg, 2010: Global warming pattern formation: Sea surface temperature and rainfall. *J. Climate*, **23**, 966–986, https://doi.org/10.1175/2009JCLI3329.1.

Yamamoto, A., H. Tatebe, and M. Nonaka, 2020: On the emergence of the Atlantic multidecadal SST signal: A key role of the mixed layer depth variability driven by North Atlantic Oscillation. *J. Climate*, **33**, 3511–3531, https://doi.org/10.1175/JCLI-D-19-0283.1.

Yashayaev, I., and J. W. Loder, 2017: Further intensification of deep convection in the Labrador Sea in 2016. *Geophys. Res. Lett.*, **44**, 1429–1438, https://doi.org/10.1002/2016GL071668.

Zhang, L., J. Li, Z. Jiang, Y. Dong, T. Ying, and Z. Zhang, 2022: Clear-sky direct aerosol radiative forcing uncertainty associated with aerosol vertical distribution based on CMIP6 models. *J. Climate*, **35**, 3021–3035, https://doi.org/10.1175/JCLI-D-21-0480.1.

Zhang, R., 2008: Coherent surface-subsurface fingerprint of the Atlantic meridional overturning circulation. *Geophys. Res. Lett.*, **35**, L20705, https://doi.org/10.1029/2008GL035463.

——, T. L. Delworth, A. Rosati, W. G. Anderson, K. W. Dixon, H.-C. Lee, and F. Zeng, 2011: Sensitivity of the North Atlantic Ocean circulation to an abrupt change in the Nordic Sea overflow in a high resolution global coupled climate model. *J. Geophys. Res.*, **116**, C12024, https://doi.org/10.1029/2011JC007240.

——, R. Sutton, G. Danabasoglu, T. L. Delworth, W. M. Kim, J. Robson, and S. G. Yeager, 2016: Comment on "The Atlantic multidecadal oscillation without a role for ocean circulation". *Science*, **352**, 1527, https://doi.org/10.1126/science.aaf1660.

——, ——, ——, Y.-O. Kwon, R. Marsh, S. G. Yeager, D. E. Amrhein, and C. M. Little, 2019: A review of the role of the Atlantic meridional overturning circulation in Atlantic multidecadal variability and associated climate impacts. *Rev. Geophys.*, **57**, 316–375, https://doi.org/10.1029/2019RG000644.